Supplement of Earth Syst. Sci. Data, 9, 281–292, 2017
http://www.earth-syst-sci-data.net/9/281/2017/
doi:10.5194/essd-9-281-2017-supplement

Supplement of

An open-access CMIP5 pattern library for temperature and precipitation: description and methodology

Cary Lynch et al.

Correspondence to: Cary Lynch (cary.lynch@pnnl.gov)

1 Supplementary Materials

1.1 Supplementary Data

Accurate simulations of observed global mean climate are not necessarily an essential pre-requisite for predicting global trends (*Rupp et al.*, 2013; *Eyring et al.*, 2016). Additionally, most modeling centers released multiple models based on different physical parameterizations and/or interactions, and the assumption of model independence is not valid (*Sanderson et al.*, 2015), and we do not assume that the models in our multi-model ensemble to be independent. To address these issues, we developed a small set of simple performance metrics based on the structure from *Rupp et al.* (2013) and compared them to the National Centers for Environmental Prediction (NCEP)/National Center for Atmospheric Research (NCAR) (*Kalnay et al.*, 1996) and the Global Precipitation Climatology Project (GPCP; (Adler et al., 2003)) reanalysis data. We then used the 'best' representative model from each modeling center, to limit the list of models used in this analysis to twelve.

Reanalysis output from the NCEP/NCAR is used to validate the model ensemble annual and seasonal climatology because it spans the later half of the 20$^{\text{th}}$ Century and has continuous spatial coverage at 2.5 x 2.5 degree resolution. It assimilates observed data into a weather prediction model at the spatial resolution of climate models and process observations in the same manner as climate models. The NCEP/NCAR reanalysis data for temperature captures observed surface temperature trends and variability reasonably well (*Simmons et al.*, 2004).

For precipitation metrics, the GPCP reanalysis was used. The GPCP data is a globally complete, monthly analysis of surface precipitation at 2.5 x 2.5 degree resolution is available from January 1979 to the present. It is a merged analysis that incorporates precipitation estimates from low-orbit satellite microwave data, geosynchronous-orbit satellite infrared data, and surface rain gauge observations.

Two global performance metrics were used: annual/seasonal climatological bias and annual/seasonal spatial correlation. To calculate annual and seasonal bias for temperature and precipitation, models were first averaged over annual or season over the historical period (1950-1999 or 1979-2008, respectively). A weighted average was then performed. Then the difference in annual/seasonal area weighted average between reanalysis datasets and all 41 models was calculated (Table 1 and 2). To calculate annual and seasonal spatial correlation for temperature and precipitation, models were first averaged over annual or season over the historical period (1950-1999 or 1979-2008, respectively). Models were then regridded to the resolution of the reanalysis data. Then the spatial pattern correlation is calculated between the reanalysis and each model. The pattern correlation is the Pearson product-moment coefficient of linear correlation between two variables at corresponding locations.

To further examine performance and to evaluate future projections we created annual/seasonal scatter plots of global mean temperature and precipitation, with the historical and rcp8.5 scenario (Supplementary Figure 1 and 2). For temperature, the models performed well as compared to reanalysis data, and the twelve member ensemble roughly captures the range of future temperature from the 41 member ensemble. For precipitation, models generally over estimated precipitation as compared to reanalysis, but clearly project an increasing trend in projected precipitation.

Analysis and plotting software for this study primarily done with the National Center for Atmospheric Research's command language.

References

Adler, R. F., Huffman, G. J., Chang, A., Ferraro, R., Xie, P.-P., Janowiak, J., Rudolf, B., Schneider, U., Curtis, S., Bolvin, D., Gruber, A., Susskind, J., Arkin, P., and Nelkin, E.: The Version-2 Global Precipitation Climatology Project (GPCP) Monthly Precipitation Analysis (1979–Present), Journal of Hydrometeorology, 4, 1147–1167, doi:10.1175/1525-7541(2003)004<1147:TVGPCP>2.0.CO;2, 2003.

Eyring, V., M. Righi, A. Lauer, M. Evaldsson, S. Wenzel, C. Jones, A. Anav, O. Andrews, I. Cionni, E. L. Davin, C. Deser, C. Ehbrecht, P. Friedlingstein, P. Gleckler, K. D. Gottschaldt, S. Hagemann, M. Juckes, S. Kindermann, J. Krasting, D. Kunert, R. Levine, A. Loew, J. Mäkelä, G. Martin, E. Mason, A. S. Phillips, S. Read, C. Rio, R. Roehrig, D. Senftleben, A. Sterl, L. H. van Ulft, J. Walton, S. Wang, and K. D. Williams (2016), ESMValTool (v1.0) –a community diagnostic and performance metrics tool for routine evaluation of Earth system models in CMIP, *Geosci. Model Dev.*, *9*(5), 1747–1802, doi:10.5194/gmd-9-1747-2016.

Kalnay, E., M. Kanamitsu, R. Kistler, W. Collins, D. Deaven, L. Gandin, M. Iredell, S. Saha, G. White, J. Woollen, Y. Zhur, M. Chelliah, W. Evisuzaki, W. Higgins, J. Janowiak, K. Mo, C. Ropelewski, J. Wang, A. Leetmaa, R. Reynolds, R. Jeene, and D. Joseph (1996), The NCEP/NCAR 40-year reanalysis project, *Bulletin of the American Meteorological Society*, *77*(3), 437 – 471.

Rupp, D. E., J. T. Abatzoglou, K. C. Hegewisch, and P. W. Mote (2013), Evaluation of CMIP5 20^{th} Century climate simulations for the Pacific Northwest USA, *Journal of Geophysical Research: Atmospheres*, *118*(19), 10,884–10,906, doi:10.1002/jgrd.50843.

Sanderson, B. M., R. Knutti, and P. Caldwell (2015), Addressing interdependency in a multimodel ensemble by interpolation of model properties, *Journal of Climate*, *28*(13), 5150–5170, doi:10.1175/JCLI-D-14-00361.1.

Simmons, A. J., P. D. Jones, V. da Costa Bechtold, A. C. M. Beljaars, P. W. Kållberg, S. Saarinen, S. M. Uppala, P. Viterbo, and N. Wedi (2004), Comparison of trends and low-frequency variability in CRU, ERA-40, and NCEP/NCAR analyses of surface air temperature, *Journal of Geophysical Research: Atmospheres*, *109* (D24), doi:10.1029/2004JD005306.

Supplementary Figures

1. Supplemental Figures 1-2

Table 1. Annual and seasonal bias and spatial correlation for surface temperature by CMIP5 model using historical simulation compared to NCEP-NCAR reanalysis (1950-1999). Bias is in ^{o}C. First twelve models are the models used in this analysis.

	ANN Bias	DJF Bias	JJA Bias	ANN Spatial Corr	DJF Spatial Corr	JJA Spatial Corr
ACCESS1-0	0.032	-0.366	0.323	0.995	0.994	0.994
CanESM2	-0.048	-0.555	0.32	0.996	0.989	0.995
CCSM4	-0.18	-0.454	0.051	0.996	0.993	0.994
CMCC-CMS	-0.077	-0.647	0.283	0.994	0.989	0.991
CNRM-CM5	-0.294	-0.771	0.272	0.993	0.992	0.989
GFDL-CM3	-0.315	-0.551	-0.205	0.994	0.993	0.991
HadGEM2-ES	-0.186	-0.847	0.301	0.994	0.991	0.992
IPSL-CM5A-MR	-0.108	-0.594	0.263	0.994	0.989	0.992
inmcm4	-0.076	-0.386	0.14	0.988	0.986	0.982
MIROC-ESM	0.082	0.24	0.061	0.994	0.99	0.993
MPI-ESM-MR	0.281	-0.277	0.486	0.995	0.988	0.99
NorESM1-m	-0.48	-0.861	-0.235	0.996	0.992	0.994
ACCESS1-3	0.245	-0.141	0.509	0.996	0.991	0.994
bcc-csm1-1	0.261	-0.076	0.302	0.993	0.991	0.992
bcc-csm1-1m	0.957	0.573	0.997	0.995	0.993	0.993
BNU-ESM	-0.448	-0.279	-0.602	0.993	0.99	0.992
CESM1-BGC	-0.069	-0.322	0.137	0.996	0.994	0.994
CESM1-CAM5	-0.691	-1.165	-0.332	0.996	0.994	0.995
CESM1-WACCM	0.071	-0.448	0.583	0.995	0.994	0.994
CMCC-CESM	-0.183	-0.765	0.198	0.991	0.992	0.989
CMCC-CM	-0.428	-1.103	0.097	0.992	0.986	0.99
CSIRO-Mk3-6-0	-1.12	-1.661	-0.732	0.994	0.99	0.994
EC-EARTH	-0.82	-1.128	-0.655	0.995	0.991	0.994
FGOALS-g2	0.03	-0.48	0.356	0.99	0.987	0.992
FIO-ESM	-0.235	-0.544	-0.15	0.993	0.992	0.992
GFDL-ESM2G	-0.382	-0.883	-0.014	0.992	0.99	0.993
GFDL-ESM2M	0.307	0.037	0.518	0.992	0.991	0.99
GISS-E2-H	1.56	1.266	1.638	0.991	0.989	0.984
GISS-E2-H-CC	0.954	0.668	1.008	0.994	0.99	0.991
GISS-E2-R	0.773	0.273	0.926	0.994	0.989	0.99
GISS-E2-R-CC	0.774	0.293	0.919	0.994	0.989	0.991
HadGEM2-AO	0.332	-0.227	0.705	0.995	0.991	0.992
HadGEM2-CC	-0.522	-1.264	0.092	0.993	0.99	0.991
IPSL-CM5A-LR	-1.031	-1.584	-0.584	0.994	0.99	0.993
IPSL-CM5B-LR	-0.484	-1.59	0.42	0.983	0.982	0.984
MIROC-ESM-CHEM	-0.025	0.169	-0.013	0.994	0.991	0.993
MIROC5	0.982	0.418	1.692	0.99	0.995	0.983
MPI-ESM-LR	0.068	-0.518	0.333	0.995	0.989	0.989
MRI-CGCM3	0.017	-0.311	0.39	0.994	0.989	0.995
MRI-ESM1	0.21	-0.087	0.544	0.993	0.989	0.995
NorESM1-ME	-0.951	-1.249	-0.747	0.996	0.992	0.993
NCEP/NCAR	0	0	0	1	1	1

Table 2. Annual and seasonal bias and spatial correlation for precipitation by CMIP5 model using historical simulation compared to GPCP reanalysis (1979-2008). Bias is in mm/month. First twelve models are the models used in this analysis.

	ANN Bias	DJF Bias	JJA Bias	ANN Spatial Corr	DJF Spatial Corr	JJA Spatial Corr
ACCESS1-0	125.172	9.504	11.376	0.884	0.869	0.841
CanESM2	10.419	0.796	1.557	0.855	0.851	0.844
CCSM4	87.971	8.03	7.805	0.882	0.883	0.853
CMCC-CMS	68.216	4.611	7.232	0.864	0.852	0.835
CNRM-CM5	113.387	9.909	9.799	0.867	0.858	0.843
GFDL-CM3	92.233	7.568	8.088	0.849	0.85	0.835
HadGEM2-ES	120.879	9.099	11.744	0.893	0.88	0.844
IPSL-CM5A-MR	32.721	2.261	3.558	0.805	0.816	0.768
inmcm4	151.956	12.252	12.83	0.805	0.838	0.736
MIROC-ESM	28.136	2.008	2.523	0.825	0.805	0.774
MPI-ESM-MR	95.583	7.422	9.58	0.825	0.81	0.81
NorESM1-m	34.283	3.291	3.367	0.855	0.842	0.812
ACCESS1-3	154.826	12.001	13.91	0.885	0.857	0.833
bcc-csm1-1	37.004	3.484	2.549	0.843	0.842	0.813
bcc-csm1-1m	54.165	5.024	4.02	0.803	0.815	0.741
BNU-ESM	129.13	11.323	9.568	0.846	0.838	0.825
CESM1-BGC	89.958	8.437	7.869	0.879	0.89	0.848
CESM1-CAM5	107.768	8.95	9.642	0.889	0.88	0.861
CESM1-WACCM	48.05	4.035	4.889	0.869	0.862	0.837
CMCC-CESM	52.439	3.413	5.926	0.809	0.824	0.745
CMCC-CM	62.634	4.212	6.994	0.859	0.839	0.821
CSIRO-Mk3-6-0	54.986	3.67	5.714	0.798	0.796	0.751
EC-EARTH	50.145	4.305	3.836	0.883	0.878	0.83
FGOALS-g2	65.589	5.061	5.646	0.85	0.853	0.779
FIO-ESM	115.952	10.111	9.211	0.846	0.813	0.807
GFDL-ESM2G	81.613	5.911	7.871	0.814	0.822	0.811
GFDL-ESM2M	90.108	7.026	8.229	0.842	0.855	0.816
GISS-E2-H	168.431	13.931	13.82	0.795	0.773	0.722
GISS-E2-H-CC	162.208	13.602	13.056	0.799	0.772	0.714
GISS-E2-R	151.245	12.171	12.68	0.827	0.806	0.768
GISS-E2-R-CC	150.63	12.057	12.666	0.828	0.803	0.768
HadGEM2-AO	133.977	11.263	8.857	0.897	0.436	0.278
HadGEM2-CC	110.105	9.451	6.906	0.89	0.429	0.292
IPSL-CM5A-LR	1.825	-0.612	1.314	0.818	0.828	0.781
IPSL-CM5B-LR	35.501	2.513	3.411	0.816	0.823	0.761
MIROC-ESM-CHEM	23.374	1.585	2.023	0.834	0.812	0.786
MIROC5	167.903	12.567	15.719	0.89	0.869	0.852
MPI-ESM-LR	80.562	6.138	8.29	0.814	0.807	0.8
MRI-CGCM3	70.826	6.819	5.686	0.826	0.803	0.798
MRI-ESM1	77.157	7.385	6.168	0.828	0.802	0.803
NorESM1-ME	25.205	2.545	2.62	0.862	0.838	0.816
GPCP	0	0	0	1	1	1

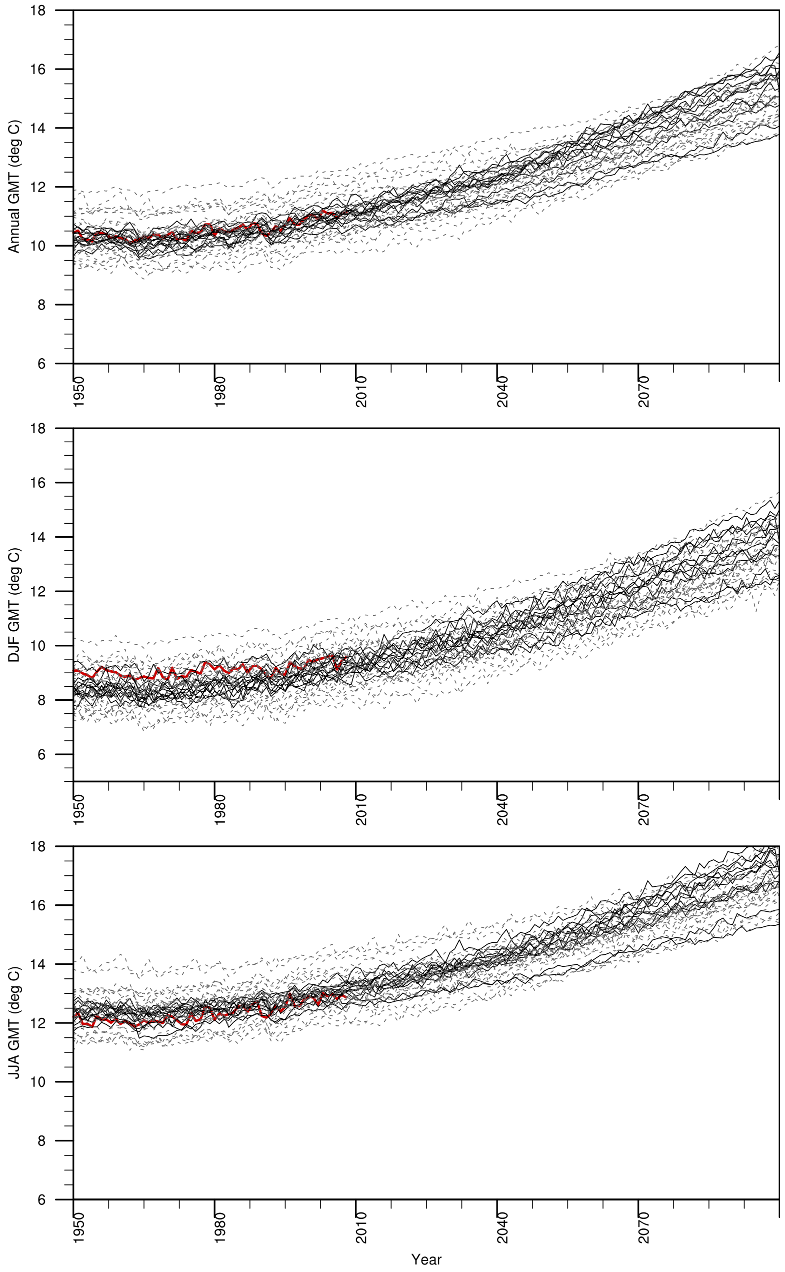

Figure 1. Reanalysis and model annual (top), December to February (middle, DJF), and June to August (bottom, JJA) mean global area weighted air temperature (^{o}C). NCEP/NCAR reanalysis (red line) compared to ensemble historical and rcp8.5 simulation (black line) for annual, DJF, and JJA. Solid black lines indicate the twelve sub-selected models used in the analysis, and dashed black lines are the 29 models not used.

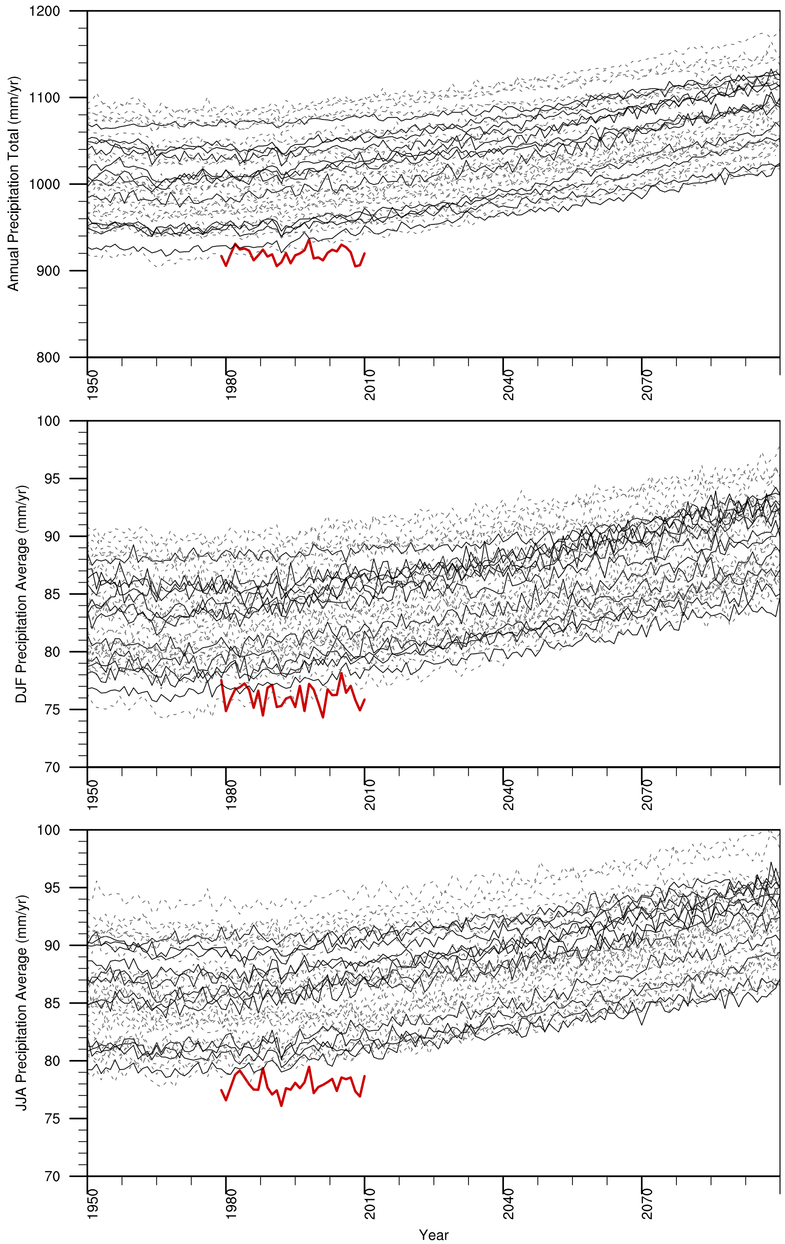

Figure 2. Reanalysis and model annual (top), December to February (middle, DJF), and June to August (bottom, JJA) mean global area weighted precipitation (mm/month). GPCP reanalysis (red line) compared to ensemble historical and rcp8.5 simulation (black line) for annual, DJF, and JJA. Solid black lines indicate the twelve sub-selected models used in the analysis, and dashed black lines are the 29 models not used.